Homotopy Particle Filter for Ground-Based Tracking of Satellites at GEO

Nima Moshtagh, Jonathan D. Chan, Moses W. Chan
Advanced Technology Center
Lockheed Martin Space Systems
Sunnyvale, CA USA

Abstract - Ground telescopes enable low-cost tracking and characterization of meter-class space objects. Since a telescope may be tasked to observe multiple fields of the sky, the time between observations for each object may vary from several seconds to tens of minutes. Long propagation times with nonlinear dynamics are challenging for traditional filtering methods such as the *Extended Kalman Filter* (EKF). Sampling-based filters based on the *Particle Filter* (PF) are promising for this type of problem but typically require maintaining a large number of samples. In this work, we evaluate the *Homotopy Particle Filter* (HPF) which promises effective performance with orders of magnitude fewer particles. The performance of the HPF is evaluated against GEO satellite observations collected by a ground telescope at Lockheed Martin's Space Object Tracking (SPOT) facility.

Keywords: Satellite tracking, state estimation, particle filtering, particle flow

1 Introduction

Space Situational Awareness (SSA) involves detecting, tracking, and characterizing resident space objects (RSO). Keeping track of RSOs in and near Geostationary Earth Orbit (GEO) is important due to the high value of GEO assets and the limited availability of GEO slots. Accurate state estimation and characterization of GEO objects is a challenging task due to the ranges involved.

Current location accuracy for objects in GEO is on the order of kilometers (~1-5 km), updated every three days [1]. Note that some orbital parameters for an object in GEO cannot be accurately estimated with one night of observation from a single stationary site. For example, offset from the nominal geosynchronous semi-major axis can only be observed with slowly-drifting azimuth measurements [2].

Another difficulty associated with tracking and characterization of RSOs in GEO occurs when multiple satellites share a single GEO slot. Typical size of a GEO slot is approximately 0.1 degrees in longitude and latitude [3]. Satellites are often separated by less than 0.05 degrees of longitude, increasing the difficulty of automated detection and characterization. Close proximity between satellites in GEO may also impact the accuracy of the general perturbation orbital elements used to identify the satellites and predict their orbits [3]. Scott and Wallace [3] studied the effectiveness of a nearest-neighbor correlation approach on co-located geostationary satellites from a ground-based optical sensor. They showed that correlation of detections to objects is practical given relatively current orbital element sets.

Ground-based telescopes such as Lockheed Martin's Space Object Tracking (SPOT) telescopes offer a low-cost capability for tracking space objects. The SPOT facility provides three 1-meter afocal telescopes on independently controlled gimbals, allowing automated tasking and tracking of multiple objects [4]. The telescopes support characterization of spectral and temporal signatures for objects in GEO. In many cases, the "spectral fingerprint" can be used to determine the type and manufacturer of the spacecraft bus [4].

This paper presents results for several nonlinear state estimation methods using SPOT telescope observations. Since a telescope may be tasked to collect observations from multiple fields of the sky, the time between observations for each object may vary from several seconds to tens of minutes. Long propagation times with nonlinear dynamics are challenging for traditional filtering methods such as the *Extended Kalman Filter* (EKF) and *Unscented Kalman Filter* (UKF) [5]. Sampling-based filters such as the *Sampling Importance Resampling Particle Filter* (SIRPF) are promising for this type of problem but typically require maintaining a large number of samples.

The objective of this work was to evaluate the performance of the *Particle Flow Filter*, also known as the *Homotopy Particle Filter* (HPF) [6]. Similar to the SIRPF, the HPF approximates densities with sets of particles and directly implements the Bayesian recursion. However, the Bayes update is computed using a particle flow rather than multiplication with a likelihood function [7]. In [8], the HPF was compared against the SIRPF in a simulated angles-only tracking scenario. In this study, the HPF is evaluated against real observations of satellites in GEO.

2 SPOT Facility

Lockheed Martin has built a Space Object Tracking (SPOT) facility in Santa Cruz, California. The facility consists of three 1-meter optical telescopes controlled by a site management system. The telescopes may be individually

or cooperatively tasked to observe space objects. The telescopes are mounted on Az-El fork mounts capable of rapid repointing and arc-second class open loop tracking. Each telescope is installed in a clamshell dome with aft-mounted benches to support additional instrument suites. The telescope domes are mounted on movable rail carts which can be arbitrarily positioned along tracks to provide variable baselines for sparse aperture imaging (see Figure 1). The telescopes achieved first light in June 2012.

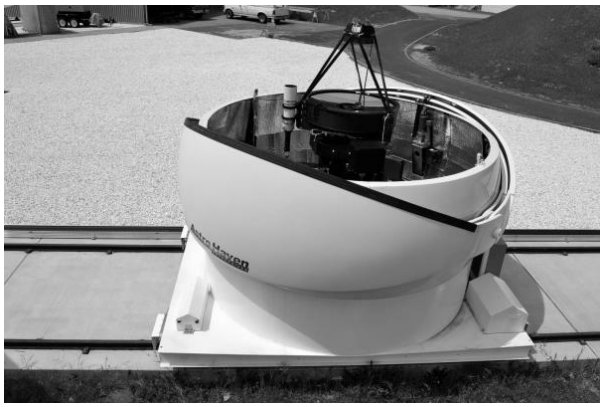

Figure 1. Photo of the SPOT telescope and mobile dome.

Typical observations consist of direct photometric imaging at visible and near-infrared wavelengths. SPOT telescopes are designed to perform the following missions [4]:

- **Space object identification**. Identifying unresolved objects using techniques such as spectroscopy, light curves, polarimetric and astrometric measurements.
- **Debris tracking**. Acquiring and tracking debris to develop accurate ephemerides.
- **Object characterization**. Exploiting photometric and spectroscopic measurements in multiple wavebands to identify constituent components and establish unique signatures for objects and classes of objects.
- **Interferometric imaging**. Leveraging interferometry to synthesize high-resolution images of objects in GEO.

2.1 Optical Sensor

The SPOT optical system consists of a primary afocal telescope with a reconfigurable backend collimator telescope and a side-mounted wide field tracker. Primary telescope properties are summarized in Table 1.

Parameter	Value
F/#	~5
Aperture Diameter	1 meter
Observation Band	Visible
Field of view (FOV)	0.25 degrees

Table 1. SPOT primary telescope optical parameters.

2.2 Data

The imagery used in this study are from a SPOT collection on the night of Oct. 13, 2014. The collection includes tasks for observing satellites in multiple fields of the sky. Therefore, there are long observation gaps for each field as the telescope observes other fields. Figure 2 shows a sample image from the data set. Each image is generated using a 3-second exposure. The streaks are caused by apparent motion of stars due to the rotation of the Earth. Streak lengths are approximately 0.0125 degrees.

A number of interesting phenomena were observed in the data. For example, there are periods of time where satellites enter the Earth's shadow, resulting in observation blackouts. In some instances with large GEO satellites, the visual magnitude of the objects can exceed the well depth of the optical sensor, causing saturation. In addition, glint from one satellite may mask a co-located GEO satellite.

During normal operations for space surveillance, the ground telescope is tasked to track a satellite which remains relatively stationary in the focal plane. Any co-located satellites appear to move relative to the tracked satellite. The apparent angular separation for co-located satellites is small when observed by a ground-based observer; occasionally the satellites may appear to conjunct despite separation in the tens of kilometers [3]. This behavior, along with observation gaps, stresses measurement correlation.

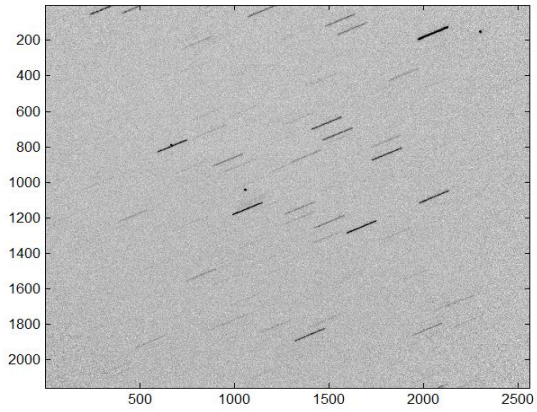

Figure 2. SPOT image with 3-second exposure time.

3 Dynamics and Measurement Models

State estimation of the satellites is performed using an Earth-Centered Inertial (ECI) coordinate frame. The x-axis is aligned with the Prime Meridian at UTC midnight for the night of observation. The z-axis is along the Earth rotation axis. The y-axis completes the right-handed coordinate frame.

3.1 Dynamics

The system state is position and velocity in the ECI coordinate frame. It is assumed the space objects obey Keplerian dynamics:

$$X_{k+1} = Kepler(X_k, dt) + w_{k:k+1}$$

where process noise $w_{k:k+1} \sim N(0, Q(dt))$ is an i.i.d. white noise capturing uncertainties in the dynamics. $Q(dt)$ is the covariance of the process noise.

Under non-linear dynamics, an initial Gaussian density will become non-Gaussian after sufficient propagation time [5]. This impacts traditional filters such as the EKF and UKF which rely on a single Gaussian to represent uncertainty. In practice, this can make it difficult to reacquire or correlate tracks after long observation gaps.

Many techniques have been explored to handle non-Gaussian densities for SSA applications, including Gaussian sum filters [5]. Our work focuses on sampling-based filters.

3.2 Detections & Measurement Model

The ground telescope supports angles-only measurements of space objects. Let X_S^{ECI} and X_T^{ECI} be the sensor and target positions in the ECI coordinate frame. The position of the space object (target) in the camera coordinate frame (CAM) is given by $X_T^{CAM} = R_{ECI}^{CAM}(X_T^{ECI} - X_S^{ECI})$, where R_{ECI}^{CAM} is the rotation matrix between ECI and CAM coordinate frames.

In this work, perspective projection was used to model sensor observations:

$$Z_k = Persp(X_T^{CAM}(k)) + n_k, \qquad (1)$$

where $n_k \sim N(0, R_k)$ is Gaussian noise representing uncertainty in the detection, and $Persp(X)$ is the observation model (perspective projection of target position $X = [x\ y\ z]$ onto the focal plane according to the camera matrix $K \in \mathbb{R}^{2x3}$):

$$Persp(X) = K\left[{}^{x}/_{z} \quad {}^{y}/_{z} \quad 1\right]'.$$

Because signal-to-noise ratio is relatively high for our targets, simple thresholding with blob characterization was adequate for generating detections from imagery.

4 Particle Filters

Particle filters approximate the optimal Bayesian filter by representing densities as sets of discrete particles with associated weights $\{x^i, w^i\}_{i=1}^N$. Formally, the posterior is represented by a discrete approximation

$$p(x_t | Z^{1:t}) \approx \sum_{i=1}^N w_t^i \delta(x_t - x_t^i),$$

Where $\delta(\cdot)$ is the Dirac delta function. As with Bayesian filtering the posterior is computed in a recursion. In the propagation step, particles are sampled from a transition density $p(x_t|x_{t-1})$ to approximate the prediction density. Given measurement z_t, the weight of each particle is updated by multiplication with a likelihood function $p(z_t|x_t^i)$ evaluated at the particle. The weights are then normalized to sum to one.

An important concern with particle filters is *sample degeneracy*. This phenomenon is characterized by very few particles having significant weight, resulting in an inefficient or inadequate sampling of the state space [7]. The *Sampling Importance Resampling* (SIR) particle filter attempts to mitigate this effect by resampling particles according to their weight.

However, resampling may lead to *sample impoverishment* where particles become too concentrated in the state space. Both degeneracy and impoverishment can be addressed by increasing the number of particles, but this approach scales poorly with state space dimensionality.

4.1 Homotopy Particle Filter

Similar to the particle filter, the HPF approximates densities as sets of discrete particles. However, instead of updating weights by multiplication with a likelihood function, the HPF implements the update as a flow of particles. The update dynamics for particles is determined by a partial differential equation (PDE). As we will see in Section 4.2, the PDE is highly under-determined, and many solutions can be found. In this work we use *Nonzero Diffusion Flow*.

To address issues with particle filters (e.g. sample degeneracy, sample impoverishment, etc.), Daum and Huang [9] proposed the *Particle Flow* or *Homotopy Particle Filter*. In the particle flow approach, particles are migrated to regions in the state space where the posterior has higher density. The particles flow progresses as a *homotopy* variable λ advances from 0 to 1.

The flow for the un-normalized posterior is generated using a homotopy

$$p(x, \lambda) = g(x) l(x)^\lambda$$

as a function of $\lambda \in [0\ 1]$. The flow of the posterior corresponds to the Bayes update. At the start of flow ($\lambda = 0$), we have $p(x, \lambda) = g(x)$, i.e. $p(x, \lambda)$ is equal to the prior density. At the end of flow ($\lambda = 1$) and $p(x, \lambda)$ is equal to the posterior density $p(x, \lambda) = g(x) l(x)$.

The flow of the logarithm of the posterior with respect to λ is given by:

$$\log p(x, \lambda) = \log g(x) + \lambda \log l(x)\,. \qquad (2)$$

This represents a *line homotopy* of the logarithm of the densities. The task is to find an appropriate flow of the probability density defined by the log-homotopy (2). Suppose the flow for the Bayes update obeys the following stochastic differential equation:

$$dx = f(x, \lambda) d\lambda + dw \qquad (3)$$

where dw is the diffusion noise with covariance matrix $Q(x)$. The objective is to compute the vector field (or flow) $f_\lambda = f(x, \lambda)$. Using the Fokker-Plank equation governing the dynamics of the posterior density, Daum and Huang [6]

derived the following first-order PDE in the unknown function f_λ:

$$\frac{\partial \log p}{\partial x} f_\lambda = -\log l - \mathrm{div}(f_\lambda) + \frac{1}{2p}\mathrm{div}\left[Q(x)\frac{\partial p}{\partial x}\right]. \qquad (4)$$

This PDE is highly under-determined because there is only one scalar-valued equation, but the unknown function $f(x,\lambda)$, or *flow*, is a D-dimensional vector field. Our objective is to solve equation (4), given $p(x,\lambda)$ and $l(x,\lambda)$. There are many solutions to this equation. In Section 4.2, a solution is derived by imposing mild assumptions on the diffusion parameter Q.

In our implementation, particles are migrated in small steps using Euler's method:

$$x^i(\lambda_k) = x^i(\lambda_{k-1}) + \Delta_k \cdot f(x^i_{k-1}, \lambda_k)\,,$$

where the step size is $\Delta_k = \lambda_k - \lambda_{k-1}$. No resampling is needed with the HPF.

4.2 HPF with Nonzero Diffusion Flow

In this section we follow the work in [9] to derive the HPF with nonzero diffusion flow. Consider the PDE (4) with unknown f_λ. Suppose the diffusion parameter Q is nonzero, and the prior density $g(x)$ and likelihood function $l(x)$ are twice differentiable. Now compute the gradient of (4) with respect to x

$$\frac{\partial \log l}{\partial x} = -f_\lambda^T \frac{\partial^2 \log p}{\partial x^2} - \frac{\partial \mathrm{div}(f_\lambda)}{\partial x} - \frac{\partial \log p}{\partial x}\frac{\partial f_\lambda}{\partial x} + \frac{\partial \mathrm{div}\left[Q(x)\frac{\partial p}{\partial x}/2p\right]}{\partial x}\,.$$

The above equation is a system of D equations with D unknown functions f_λ. If a nonzero diffusion Q and flow f_λ exist such that the last three terms are summed up to zero, we arrive at the simpler equation:

$$\left(\frac{\partial \log l}{\partial x}\right) = -f_\lambda^T \left(\frac{\partial^2 \log p}{\partial x^2}\right). \qquad (5)$$

Then, under the stated assumptions, the unique solution for f_λ is given by:

$$f_\lambda = -\left(\frac{\partial^2 \log p}{\partial x^2}\right)^{-1}\left(\frac{\partial \log l}{\partial x}\right)^T. \qquad (6)$$

If the likelihood function l is known analytically, the derivative of $\log l$ can be computed analytically as well. To compute the Hessian of $\log p$, the definition of log-homotopy (2) is used:

$$\frac{\partial^2 \log p}{\partial x^2} = \frac{\partial^2 \log g}{\partial x^2} + \lambda\,\frac{\partial^2 \log l}{\partial x^2}\,. \qquad (7)$$

The Hessian of $\log l$ is computed in closed-form, but computing the Hessian of $\log g$ is more difficult. An approach using the k-nearest neighbor algorithm was proposed in [10]. The Hessian of $\log p$ is also known as the *Observed Fisher Information Matrix*.

If a Gaussian approximation to g is used, the Hessian of $\log g$ can be approximated by the sample covariance matrix P_s of the prior computed from the particles at $\lambda = 0$. For applications where the nonlinear measurement has additive Gaussian noise, the information matrix (Hessian of $\log p$, evaluated at x^i) becomes

$$I(x^i,\lambda) = \frac{\partial^2 \log p}{\partial x^2}\Big]_{x^i} = -P_s^{-1} - \lambda H(x^i)^T R^{-1} H(x^i)\,.$$

Using (6), the nonzero diffusion flow of each particle becomes

$$f_\lambda(x^i) = -I(x^i,\lambda)^{-1} H(x^i)^T R^{-1}(z - h(x^i)), \qquad (8)$$

where $H(x^i)$ is the linearized measurement matrix evaluated at x^i and R is the measurement noise covariance. Note that this is similar to the *Extended Information Filter* [11] but for each particle rather than the conditional mean.

5 Implementation and Results

The following filters were implemented in MATLAB:

- HPF with nonzero diffusion flow
- SIRPF
- EKF

The filters were updated with detections from SPOT imagery collected on the night of Oct. 13, 2014.

The HPF and SIRPF were initialized with samples drawn uniformly from a cubic volume `200 x 200 x 200` km centered on the intersection of the sensor line-of-sight and the GEO belt. Sample velocities were drawn uniformly from the interval `[-100, +100]` m/sec centered on nominal GEO speed (`~3.07` km/sec). The EKF was initialized with a Gaussian matching the first and second moments of the HPF and SIRPF prior.

5.1 Effects of Number of Particles

Our interest was evaluating the claim of HPF requiring orders of magnitude fewer particles than SIRPF. We evaluate state estimation accuracy for HPF and SIRPF parameterized by number of particles. Our metric for state estimation accuracy was error between the prediction density mean and the measurement centroid. This metric provides an indication for how each filter might support reacquisition and association of a target after long observation gaps.

Figure 3 illustrates temporal behavior of prediction error for an observed field. The saw-tooth pattern highlights the growth of state estimation error during observation gaps. Note the lack of a pronounced saw-tooth for the SIRPF with 10000 particles. This is caused by poor sampling of the state

space reducing information gain from measurements. SIRPF requires 2 million particles before approaching the performance of HPF with 100 particles.

Figure 4 shows prediction error following the first observation gap. HPF error converges quickly with number of particles, but SIRPF requires more than 100000 particles before error begins to drop significantly. For reference, a thresholded detection is approximately 10 pixels in diameter.

Figure 5 shows mean processing time for each filter, normalized by the processing time of EKF. For the same number of particles, the HPF implementation requires approximately two orders of magnitude more processing time than SIRPF. But for the same or better prediction error, HPF requires about four orders of magnitude fewer particles.

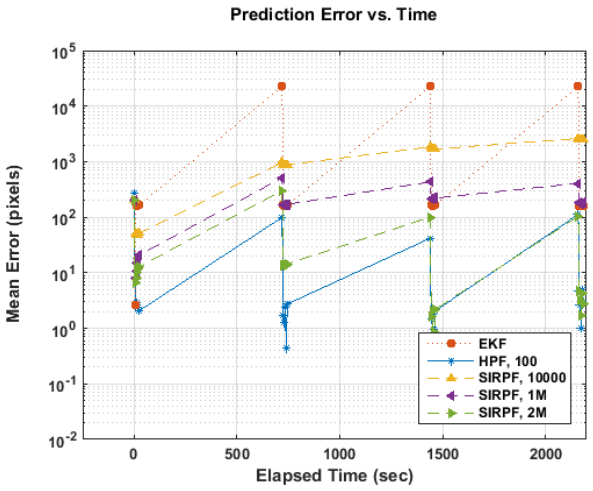

Figure 3. Prediction error over time for EKF, HPF, and SIRPF. Time between measurements is 5 seconds. Observation gap is 11.5 minutes.

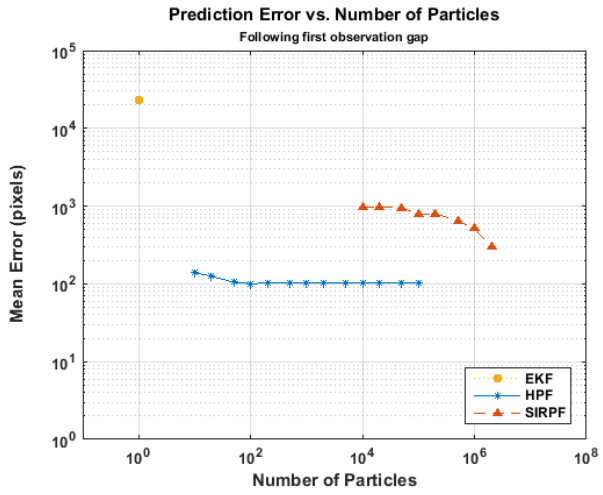

Figure 4. Prediction error versus number of particles for EKF, HPF, and SIRPF after the first observation gap.

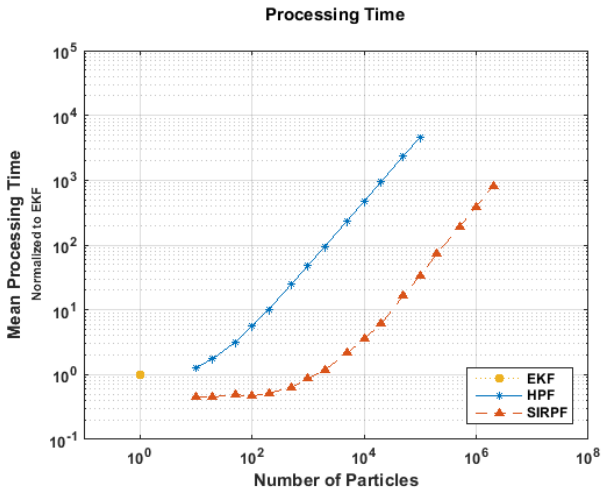

Figure 5. Processing time versus number of particles for EKF, HPF, and SIRPF, normalized to EKF processing time.

6 Conclusions

- HPF and SIRPF (with an adequate number of particles) both outperform EKF since they are better able to represent uncertainty through longer observation gaps.
- HPF requires orders of magnitude fewer particles than SIRPF for similar or better prediction error.
- HPF with nonzero diffusion flow requires linearization of the measurement model for each particle which increases computational cost per particle.
- HPF with nonzero diffusion flow requires fine integration steps for particle flow which increases computational cost per particle.

7 Acknowledgements

The authors would like to thank Michael Marinos for his support in providing data and technical guidance.

References

[1] T. Blake, M. Sánchez, J. Krassner, M. Georgen and S. Sundbeck., "Space Domain Awareness," in *AMOS Conference*, Maui, HI, 2012.

[2] J. Tombasco and P. Axelrad, "A study of the achievable geosynchronous angles-only orbit estimation accuracy," in *The Journal of the Astronautical Sciences 58.2*, 2011, pp. 275-290.

[3] R. Scott and B. Wallace, "Small aperture telescope observations of co-located geostationary satellites," in *AMOS Technical Conference Proceedings*, 2009.

[4] R. Shivitz, R. Kendrick, J. Mason, M. Bold, T. Kubo, K. Bock and D. Tyler, "Space Object Tracking (SPOT) facility," in *SPIE Astronomical Telescopes+*

Instrumentation, International Society for Optics and Photonics, 2014, pp. pp. 91450J-91450J.

[5] J. T. Horwood, N. D. Aragon and A. B. Poore, "Gaussian sum filters for space surveillance: theory and simulations," *Journal of Guidance, Control, and Dynamics,* vol. 34, no. 6, pp. 1839-1851, 2011.

[6] F. Daum and J. Huang, "Particle flow for nonlinear filters with log-homotopy," in *Proceedings of SPIE Signal Processing, Sensor Fusion, and Target Recognition XVIII*, 2009, p. 733603.

[7] F. Daum and F. Haung, "Particle Degeneracy: root cause and solution," in *Proceedings of SPIE 8050, Signal Processing, Sensor Fusion, and Target Recognition XX*, Orlando, Florida, USA, 2011, p. 80500W.

[8] N. Moshtagh and M. W. Chan, "Multisensor fusion using homotopy particle filter," in *18th International Conference on Information Fusion (Fusion)*, IEEE, 2015.

[9] F. Daum and J. Huang, "Particle flow with nonzero diffusion for nonlinear filters," in *Proceedings of SPIE: Signal processing, sensor fusion and target tracking XXII*, Baltimore, MD, 2013, p. 87450P.

[10] F. Daum, J. Huang, A. Noushin and M. Krichman, "Gradient estimation for particle flow induced by log-homotopy for nonlinear filters," in *Proceedings of SPIE 7336, Signal Processing, Sensor Fusion, and Target Recognition XVIII*, 2009, p. 733602 .

[11] H. Durrant-Whyte and T. C. Henderson, "Multisensor data fusion," in *Springer Handbook of Robotics*, Springer, 2008, pp. 585--610.

[12] S. Godsill and T. Clapp, "Improvement strategies for particle filters," in *Sequential Monte Carlo Methods in Practice*, Springer-Verlag, 2001, pp. 139-158.

[13] B. K. Bradley and P. Axelrad, "Improved estimation of orbits and physical properties of objects in GEO," in *Advanced Maui Optical and Space Surveillance Technologies Conference (AMOS)*, Maui, HI, 2013.

[14] C. Sabol and R. Culp, "Improved angular observations in geosynchronous orbit determination," in *Journal of Guidance, Control, and Dynamics 24.1*, 2001, pp. 123-130.